Available online at www.sciencedirect.com
ScienceDirect
Journal of Sound and Vibration 302 (2007) 208–228
JOURNAL OF SOUND AND VIBRATION
www.elsevier.com/locate/jsvi

Acoustic resonance scattering from a submerged functionally graded cylindrical shell

Seyyed M. Hasheminejad*, M. Rajabi

Acoustics Laboratory, Department of Mechanical Engineering, Iran University of Science and Technology, Narmak, Tehran 16844, Iran

Received 8 June 2006; received in revised form 25 September 2006; accepted 21 November 2006
Available online 11 January 2007

Abstract

An exact treatment based on the inherent background coefficients that describe the background amplitudes in the scattered field is employed to investigate the scattering of time-harmonic plane acoustic waves by an arbitrarily thick hollow isotropic functionally graded cylinder submerged in and filled with non-viscous compressible fluids. The mechanical properties of the graded shell are assumed to vary smoothly and continuously with the change of volume concentrations of the constituting materials (ZrO_2 and Al) across the thickness of the shell according to a power-law distribution. The original inhomogeneous shell is approximated by a laminate model, for which the solution is expected to gradually approach the exact one as the number of layers increases. The transfer matrix (*T*-matrix) solution technique, which involves a system global transfer matrix formed as the product of the individual transfer matrices by applying continuity of the displacement and stress components at the interfaces of neighbouring layers, is employed to solve for the modal scattering coefficients. Following the classic acoustic resonance scattering theory (RST), the scattered field and response to surface waves are determined by constructing the partial waves and obtaining the backgrounds (non-resonance) and resonance components from it. Three types of FGM cylindrical shells composed of Al and ZrO_2 are configured and their response spectra to an incident plane wave are calculated. The effects of the FGM interlayer thickness and material compositional gradient (the constituent volume fraction) on the inherent background, global and resonance scattering coefficients are examined. Limiting cases are considered and good agreements with the solutions available in the literature are obtained.

1. Introduction

In recent years, the study of functionally graded materials (FGMs) has attracted a lot of attention. FGMs are advanced composites, microscopically engineered to have a smooth spatial variation of material properties in order to improve overall performance. This is achieved by fabricating the composite material to have a gradual spatial variation in the constituent materials' relative volume fractions and microstructure; thus, tailoring its material composition based on functional performance requirements [1,2]. The concept of FGM was first introduced in 1984 by a group of material scientists in Japan [3] as an alternative to laminated

*Corresponding author. Tel.: +9821 73912936; fax: +9821 7451143.
E-mail address: hashemi@iust.ac.ir (S.M. Hasheminejad).

0022-460X/$ - see front matter © 2006 Elsevier Ltd. All rights reserved.
doi:10.1016/j.jsv.2006.11.014

Nomenclature

a_j outer radius of the jth layer in the FGM shell

c_1, c_2 speeds of sound in the outer and inner fluid mediums

f_n global scattering coefficient for the nth mode

f_∞ backscattering form-function amplitude

$f_n^{(b)}$ inherent background coefficient for the nth mode

$f_n^{(\mathrm{res})}$ resonance scattering coefficient for the nth mode

j layer number in the FGM shell

k_1, k_2 wavenumbers in the outer and inner fluid mediums

$k_p^{[j]}$, $k_s^{[j]}$ compressional and shear elastic wavenumbers the jth layer of the FGM shell

h_j thickness of the jth layer in the FGM shell

h_I thickness of the FGM interlayer

n mode number

p_1, p_2 acoustic pressures in the outer and inner fluid mediums

q total number of layers in the FGM shell

r radial coordinate in the polar coordinate system

$\bar{r}_j$ mean radius of the jth layer in the FGM shell

$\mathbf{u}$ displacement vector in the FGM shell

$u_r^{[j]}$, $u_\theta^{[j]}$ radial and tangential displacement components in the jth layer of the FGM shell

$u_{r,n}^{[j]}$, $u_{\theta,n}^{[j]}$ modal amplitudes of the radial and tangential displacement components in the jth layer of the FGM shell

$\mathbf{v}$ fluid particle velocity vector

$\mathbf{v}_r$ radial component of the fluid particle velocity vector

x, y, z Cartesian coordinate system

A_n scattering coefficient in the outer fluid medium

$A_n^{(b)}$ background scattering coefficient

B_n transmission coefficient in the inner fluid medium

$C_n^{[j]}$, $D_n^{[j]}$, $E_n^{[j]}$, $G_n^{[j]}$ transmission coefficients in the jth layer of the FGM shell

$[F_n(0^+)]_j$ zero limit of the modal accelerance function associated with the jth layer of the FGM shell

$H_n^{(1)}$, $H_n^{(2)}$ cylindrical Hankel functions of the first and second kind of order n

J_n cylindrical Bessel function of the first kind of order n

$\mathbf{Q}_n^{[j]}$ coefficient matrix relating the modal field variables (stress and displacements) to the transmission coefficients in the jth layer of the FGM shell (see Appendix A)

$\mathbf{M}_n^{[j]}$ local transfer matrix for the jth layer of the FGM shell

$\mathbf{T}_n$ global transfer matrix for the FGM shell

V_F volume fraction function of the metallic constituent (Aluminium)

$\mathbf{W}_n^{[j]}$ field variable vector containing the modal stress and displacement components

$\mathbf{X}^{[j]}$ amplitude vector containing the transmission coefficients in the jth layer of the FGM shell

Y_n cylindrical Bessel function of the second kind of order n

γ exponent coefficient associated with the power-law variation in the volume fraction function of the metallic constituent

δ dilatation of the elastic medium ($=\nabla\cdot\mathbf{u}$)

ε_n Neumann factor

φ_0 incident wave velocity potential amplitude

φ_1, φ_2, $\varphi_{\mathrm{inc.}}$ velocity potentials associated with the acoustic waves scattered from, transmitted into, and incident upon the FGM shell

$\lambda_s^{[j]}$, $\mu_s^{[j]}$ Lame constants for the jth layer of the FGM shell

θ angular coordinate in the polar coordinate system

ρ_1, ρ_2 mass density of the outer and inner fluid mediums

$\rho_s^{[j]}$ mass density of the jth layer in the FGM shell

$\sigma_{rr}^{[j]}$, $\sigma_{r\theta}^{[j]}$ radial and shear stress components in the jth layer of the FGM shell

$\sigma_{rr,n}^{[j]}$, $\sigma_{r\theta,n}^{[j]}$ modal amplitudes of the radial and shear stress components in the jth layer of the FGM shell

ϕ_j displacement potential representing the compressional waves in the jth layer of the FGM shell

ψ_j displacement potential representing the shear waves in the jth layer of the FGM shell

ω circular frequency

composite materials which show a mismatch in properties at material interfaces. FGMs offer great promise in applications where the operating conditions are severe, including spacecraft heat shields (thermal barrier structures), heat exchanger tubes, biomedical implants, flywheels, fusion reactors, blades, storage tanks, pressure vessels, and general wear and corrosion resistant coatings or for joining dissimilar materials in aerospace, automobile and defence industries. A review on various aspects of FGMs can be found in the monographs by Suresh and Mortensen [4] and Miyamoto et al. [5].

As the dynamic parameters play an important role in the design of modern advanced structures, a relatively large number of investigations on dynamic characteristics of inhomogeneous structures and in particular FGM cylindrical shells can be found in the literature. The important contributions are cited here. Loy et al. [6] employed Love's shell theory and the Rayleigh–Ritz method to examine free vibrations (natural frequencies) of simply supported FGM cylindrical shells composed of stainless steel and nickel. This work was later extended to the cylindrical shells with various boundary conditions [7]. Gong et al. [8] used Reddy's third-order shear deformation theory (without incorporating transverse normal deformation) to present an analytic solution to predict the transient response of simply supported FGM cylindrical shells subjected to low-velocity impact by a solid striker. Ng et al. [9] studied dynamic instability of simply supported FGM cylindrical shells under harmonic axial loading by using a normal-mode expansion and Bolotin's method to determine the boundaries of the unstable regions. Han et al. [10] presented a hybrid numerical method (HNM), which combines the finite element method with the Fourier transformation method, to analyse transient waves in an FGM cylinder subject to a radial line load acting on its outer surface. Han and Liu [11] subsequently extended the latter approach for analysing dispersion and characteristics of surface waves in a circular cylinder composed of functionally graded piezoelectric material (FGPM). Also, Han et al. [12] employed Fourier transformation and modal analysis to propose a numerical method for analysing transient waves in cylindrical shells of an FGM excited by impact point loads. Yang and Shen [13] used Reddy's higher-order shear deformation shell theory to investigate free vibration and dynamic instability of functionally graded cylindrical panels subjected to thermo-mechanical loads consisting of a steady temperature change, static and periodically pulsating forces in axial direction. Sofiyev [14] applied Galerkin's method in combination with a Ritz-type variational approach to study buckling of cylindrical thin FGM shells made of FGM composed of ceramic and metal subjected to external pressure varying as a power function of time. Subsequently, Sofiyev [15] applied Galerkin's method along with Lagrange–Hamilton principle to provide an analytic solution for the stability behaviour of compositionally graded ceramic-metal cylindrical shells under aperiodic axial compressive loading. Three-dimensional (3-D)solutions were presented by Chen and co-workers, who investigated free vibration of an orthotropic FGM cylindrical shell [16] and also a functionally graded piezoelectric hollow cylinder [17], both filled with a non-viscous compressible fluid medium. Elmaimouni et al. [18] made use of Legendre polynomials and harmonic functions to develop a numerical method for calculating guided wave propagation in an FGM infinite cylinder. Zhu et al. [19] presented a 3-D theoretical analysis of the dynamic instability of functionally graded piezoelectric circular cylindrical shells subjected to a combined loading of periodic axial compression and electric field in the radial direction. Patel et al. [20] analysed the free vibration characteristics of functionally graded elliptical cylindrical shells using finite element formulated based on the high order shear deformation theory. Just recently, Kadoli and Ganesan [21] presented linear (LN) thermal buckling and free vibration analysis for functionally graded cylindrical shells with clamped–clamped boundary condition based on temperature-dependent material properties. Pelletier and Vel [22] used the 3-D steady-state heat conduction and thermoelasticity equations, simplified for the case of generalized plane strain deformations in the axial direction, to present an exact solution for the steady-state response of a functionally graded thick cylindrical shell subjected to thermal and mechanical loads. Shakeri et al. [23] employed Galerkin finite element and fast Fourier transform (FFT) methods to present an analysis for the dynamic response of a functionally graded thick hollow cylinder in plane strain condition subjected to axisymmetric dynamic loading.

The resonances of an elastic object are considered as its fingerprints. They are intrinsic characteristics of the object, which are completely independent of the source of excitation and depend only on its bulk physical properties (e.g., bulk density and elastic constants). The resonance effects may be caused by the excitation of eigenvibrations of an elastic component by an incident acoustic wave. When an elastic target is insonified by an acoustic wave, a geometric reflection is returned from the target and various types of surface waves are

generated in the surrounding fluid medium as well as inside the target. The scattered pressure field from the target contains valuable information about the characteristics of the target and the surrounding medium. Appropriate exploitation of this information and proper identification of the resonance frequencies of the elastic object can serve as a powerful tool in many applications such as material characterization and non-destructive testing of materials [24,25], remote classification of submerged targets [26,27], and on-line monitoring of elastic components [28].

Resonance scattering theory (RST) was first introduced by Flax et al. [29] who applied the resonance formalism of nuclear-reaction theory to the problem of sound scattering from submerged elastic bodies like circular cylinders and spheres. They demonstrated that the strongly fluctuating behaviour of the scattered signal is caused by a superposition of generally narrow resonances in the individual normal modes and a background of rigid or soft-body scattering. They also showed that for scattering at a frequency in between two eigenfrequencies of the elastic body, the scatterer appears as an impenetrable object. Conversely, at and near an eigenfrequency, a scattering resonance is excited by the incident wave. Numerous authors have investigated resonance scattering by submerged cylindrical shells. Murphy et al. [30] extended the RST, developed for acoustic wave scattering from elastic objects and elastic-wave scattering from cavities, to the problem of sound scattering from fluid-filled elastic cylindrical shells in a fluid. Gaunaurd and Brill [31] used RST to investigate scattering by an air-filled hollow elastic cylinder excited by an incident plane acoustic wave. They presented accurate expressions for the phase and group velocities and for the phase and group attenuations of the first few surface waves circumnavigating (the extreme cases of) rigid and soft cylinders. Izbicki et al. [32] used RST to investigate the effect of the natural modes associated with the circumferential (axial) waves which propagate around (along) the tube (axis) on scattering of an acoustic wave by an elastic circular cylindrical shell immersed in water and obtained good agreement between the RST predictions and experimental results. Talmant et al. [33] employed spectral decomposition of the multiple echo pulses using the Numrich–de Billy method and subsequent RST analysis to present an experimental and theoretical study of the properties of circumferential waves on thin-walled elastic, air-filled cylindrical shells immersed in water. Veksler [34] considered the two-dimensional (2-D) problem of the scattering of a plane acoustic pressure wave by an empty cylindrical shell and showed that besides the specularly reflected and the diffracted waves, Lamb-type waves contribute to the frequency dependence. Izbicki et al. [35] used RST to calculate the frequency resonances and their width related to Scholte–Stoneley waves propagating around circular cylindrical shells (air-filled aluminium pipes) of different thickness ratios. These waves are known to propagate around circular cylindrical shells with a phase velocity that is less than the phase velocity of sound in water. Maze et al. [36,37] also examined resonances of the fluid-borne Scholte–Stoneley circumferential wave propagating around an evacuated cylindrical shell immersed in water. Talmant and Batard [24] considered the resonant scattering of a plane acoustical wave in normal incidence by penetrable cylinders and tubes and numerically investigated the dependence of the resonance parameters (frequency and width) on the bulk properties of the scatterer (density, shear and longitudinal velocities). Kaduchak and Loeffler [38] analysed backscattering effects due to filling the interior cavity of a submerged cylindrical shell with a higher impedance fluid such as water. Maze et al. [39] examined the helical wave resonances (i.e., the circumferential, the transversal guided, and the Scholte waves) observed in the scattered echoes obtained from an infinite pipe insonified with a plane short pulse in oblique incidence. Liu and Tang [40] derived a simple and explicit expression for the purely elastic resonance scattering function associated with oblique incidence of a plane acoustic wave on a submerged aluminium cylindrical shell of infinite length. Lee et al. [41] introduced complex wavenumbers to investigate the effects of material attenuation on acoustic resonance scattering from cylindrical shells for the purpose of applying it to ultrasonic non-destructive evaluation (NDE). Veksler and Izbicki [42] proposed a procedure for modal resonance isolation in the scattering problems of a plane acoustic wave by cylindrical and spherical shells. Kaduchak and Loeffler [43] used the exact 3-D elasticity theory to examine acoustic scattering from a multilayered transversely isotropic cylindrical shell excited by an obliquely incident plane wave. Choi et al. [44–46] considered resonance scattering of acoustic waves from submerged penetrable targets of canonical geometry (e.g., an empty cylindrical or spherical elastic shell in a fluid) and proposed exact expressions, named the inherent background coefficients, which is obtained from the zero-frequency limit of an equivalent fluid target, in order to properly describe the acoustical background over the entire frequency range. Joo et al. [47] subsequently extended the concept of the inherent background to multilayered elastic cylindrical structures by

solving the problem of acoustic wave scattering by an analogous liquid structure. Conoir et al. [48] studied the resonances of an air-filled elastic cylindrical shell immersed in a fluid using the phase gradient method, which is based on the phase derivative of the scattering matrix with regard to the frequency. Kheddioui et al. [49] theoretically and experimentally studied resonant scattering by a pair of parallel elastic cylindrical shells immersed in water. They evaluated the strength of the multiple interaction couplings between the two shells in relation to the gap between them. Bao et al. [50] used partial-wave resonances in the acoustic scattering amplitude of a normally incident plane wave to discuss the existence of various types of circumferential waves, both predominantly shell or fluid borne, for an infinite, thin elastic, circular-cylindrical shell immersed in a fluid and filled with another fluid. Tesei et al. [26] used resonance scattering analysis based on autoregressive (AR) spectral estimation technique to characterize and classify submerged elastic targets (e.g., water-loaded elastic, cylindrical, thin-walled shells immersed in salt water) in terms of their elastic and geometrical parameters. More recently, Überall [51] reviewed the physical phenomena that arise in the scattering of acoustic waves from fluid-immersed elastic (metallic spherical and cylindrical) shells which may be either evacuated or filled with the same or with a different fluid. He discussed the various phenomena occurring including the formation of circumferential (peripheral or "surface") waves t hat circumnavigate the shells, propagating either as elastic waves in the shell material or as fluid-borne waves of the Scholte–Stoneley type in the external or the internal fluid. Kim and Ih [52] used the normal mode expansion technique to present a resonance scattering analysis for obliquely incidence of a plane acoustic wave upon an air-filled, transversely isotropic cylindrical shell immersed in water. In a much related problem, Fan et al. [53] studied the circumferential resonance modes of an immersed solid elastic cylinder which is insonified by an obliquely incident plane acoustic wave over a large range of incidence angles. They employed RST to derive physical explanations for singular features of their frequency-incidence angle plots.

The above review clearly indicates that, in contrast with the homogeneous shells, there seem to be no rigorous investigations on acoustic interaction of an incident wave field with a functionally graded cylindrical shell. The primary purpose of the current work is to fill this gap. Consequently, we employ the novel features of RST in combination with the classical T-matrix solution approach [54] to carry out an exact analysis for scattering of acoustic waves by a thick-walled functionally graded hollow cylinder submerged in and filled with compressible ideal fluids. The proposed model is of high practical value in ultrasonic characterization or testing of FGM cylindrical vessels, storage tanks, and pipelines which are of important application in oil, gas, water transport, power generation, and chemical processing industries [1–5,24,25]. It is also of interest in other closely related technical applications such as remote classification of submerged targets (shells) [26,27] or on-line monitoring of elastic components [28] fabricated from FGMs.

2. Acoustic mediums

Following the standard methods of theoretical acoustics, the field equations for an inviscid and ideal compressible medium that can not support shear stresses may conveniently be expressed in terms of a scalar velocity potential as [55]

$$\mathbf{v} = -\nabla\varphi, \quad p = -\mathrm{i}\omega\rho\varphi, \quad \nabla^2\varphi + k^2\varphi = 0, \tag{1}$$

where $k = \omega/c$ is the wavenumber for the dilatational wave, c the speed of sound, ρ the ambient density, $\mathbf{v}$ the fluid particle velocity vector, and p the acoustic pressure. Also, noting that the incident wave is time-harmonic, with the circular frequency ω, we have assumed harmonic time variations throughout with the $\mathrm{e}^{-\mathrm{i}\omega t}$ dependence suppressed for simplicity.

The dynamics of the problem may be expressed in terms of appropriate scalar potentials that can be represented in the form of an infinite generalized Fourier series whose unknown scattering coefficients are to be determined by imposing the proper boundary conditions. The problem geometry is depicted in Fig. 1, where (x, y, z) is the Cartesian coordinate system with origin at O, the z direction is coincident with the axis of the cylindrical shell, and (r, θ) is the corresponding cylindrical polar coordinate system. The expansion of the

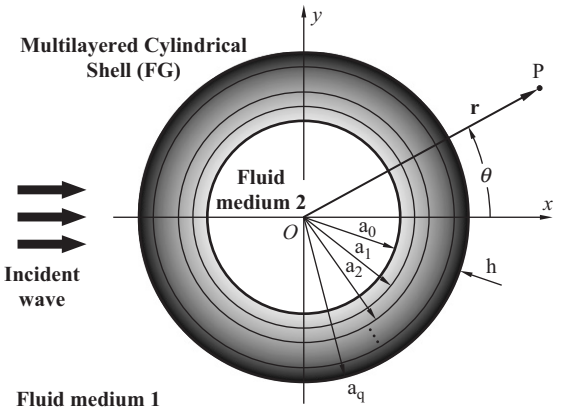

Fig. 1. Problem geometry.

incident plane wave in cylindrical coordinate has the form [56]

$$\varphi_{\text{inc.}}(r,\theta,\omega) = \varphi_0 \sum_{n=0}^{\infty} \varepsilon_n \mathrm{i}^n J_n(k_1 r)\cos(n\theta), \tag{2}$$

where J_n is the cylindrical Bessel function of the first kind of order n [57], symbol ε_n the Neumann factor ($\varepsilon_n = 1$ for $n = 0$, and $\varepsilon_n = 2$ for $n > 0$), $\mathrm{i} = \sqrt{-1}$, φ_0 the amplitude of the incident wave, $k_1 = \omega/c_1$ is the wavenumber in the medium 1 (see Fig. 1), and the subscripts 1 and 2 for the material properties refer to the surrounding and the inner fluid mediums, respectively, throughout the formulation. Likewise, keeping in mind the radiation condition, the solutions of the Helmholtz equation for the scattered potential in the surrounding fluid medium 1 and the transmitted potential in the encapsulated fluid medium 2 can, respectively, be expressed as an linear combination of cylindrical waves as [56]

$$\begin{aligned}\varphi_1(r,\theta,\omega) &= \sum_{n=0}^{\infty} \varepsilon_n \mathrm{i}^n A_n(\omega) H_n^{(1)}(k_1 r)\cos(n\theta),\\ \varphi_2(r,\theta,\omega) &= \sum_{n=0}^{\infty} \varepsilon_n \mathrm{i}^n B_n(\omega) J_n(k_2 r)\cos(n\theta),\end{aligned} \tag{3}$$

where $k_2 = \omega/c_2$ is the acoustic wavenumber in the medium 2, $H_n^{(1)}(x) = J_n(x) + \mathrm{i}\,Y_n(x)$ is the cylindrical Hankel function of the first kind of order n, $Y_n(x)$ is the cylindrical Bessel function of the second kind of order n [57], and A_n and B_n are unknown coefficients. Furthermore, using Eq. (1), the radial velocities and acoustic pressures in mediums 1 and 2 are, respectively, written as

$$\begin{aligned}\mathbf{v}_r^{(1)} &= -\frac{\partial(\varphi_{\text{inc.}} + \varphi_1)}{\partial r} = \sum_{n=0}^{\infty}\left[-\varphi_0 k_1 \varepsilon_n \mathrm{i}^n J_n'(k_1 r) - k_1 \varepsilon_n \mathrm{i}^n H_n^{(1)'}(k_1 r) A_n(\omega)\right]\cos(n\theta),\\ \mathbf{v}_r^{(2)} &= -\frac{\partial \varphi_2}{\partial r} = -\sum_{n=0}^{\infty} k_2 \varepsilon_n \mathrm{i}^n J_n'(k_2 r) B_n(\omega)\cos(n\theta)\end{aligned} \tag{4a}$$

and

$$\begin{aligned}p_1 &= -\mathrm{i}\omega\rho_1(\varphi_{\text{inc.}} + \varphi_1) = \sum_{n=0}^{\infty}\left[-\omega\rho_1\varphi_0\varepsilon_n \mathrm{i}^{n+1} J_n(k_1 r) - \omega\rho_1\varepsilon_n \mathrm{i}^{n+1} H_n^{(1)}(k_1 r) A_n(\omega)\right]\cos(n\theta),\\ p_2 &= -\mathrm{i}\omega\rho_2\varphi_2 = -\sum_{n=0}^{\infty} \omega\rho_2\varepsilon_n \mathrm{i}^{n+1} J_n(k_2 r) B_n(\omega)\cos(n\theta),\end{aligned} \tag{4b}$$

where prime denotes differentiation with respect to the argument.

3. Elastic shell

The wave motion in an isotropic elastic medium is governed by the classical Navier's equation [58]

$$\rho_s \frac{\partial^2 \mathbf{u}}{\partial t^2} = \mu_s \nabla^2 \mathbf{u} + (\lambda_s + \mu_s)\nabla(\nabla \cdot \mathbf{u}) \tag{5}$$

subject to the appropriate boundary conditions. Here, ρ_s is the solid material density, λ_s, μ_s are the Lame constants, and $\mathbf{u}$ is the vector displacement that can advantageously be expressed as sum of the gradient of a scalar potential and the curl of a vector potential:

$$\mathbf{u} = \nabla \boldsymbol{\phi} + \nabla \times \boldsymbol{\psi} \tag{6}$$

with the condition $\nabla \cdot \boldsymbol{\psi} = 0$ [58]. Furthermore, by making use of problem symmetry (see Fig. 1), we have $\boldsymbol{\psi} = (0, 0, \psi)$ [56]. The above decomposition enables us to separate the dynamic equation of motion into the classical Helmholtz equations:

$$(\nabla^2 + k_p^2)\phi = 0, \quad (\nabla^2 + k_s^2)\psi = 0, \tag{7}$$

where k_p and k_s are complex wavenumbers, known as [58]

$$k_p = \frac{\omega}{\sqrt{(\lambda_s + 2\mu_s)/\rho_s}}, \quad k_s = \frac{\omega}{\sqrt{\mu_s/\rho_s}}. \tag{8}$$

The displacement components of the elastic medium in the polar coordinate system are [58]

$$u_r = \frac{\partial \phi}{\partial r} + \frac{1}{r}\frac{\partial \psi}{\partial \theta}, \quad u_\theta = \frac{1}{r}\frac{\partial \phi}{\partial \theta} - \frac{\partial \psi}{\partial r} \tag{9}$$

and the radial and tangential stresses may be written as

$$\sigma_{rr} = \lambda_s \delta + 2\mu_s \frac{\partial u_r}{\partial r}, \quad \sigma_{r\theta} = \mu_s \left(\frac{1}{r}\frac{\partial u_r}{\partial \theta} + \frac{\partial u_\theta}{\partial r} - \frac{u_\theta}{r} \right), \tag{10}$$

where $\delta = \nabla \cdot \mathbf{u} = \nabla^2 \phi = -k_p^2 \phi$.

Now, we consider a functionally graded cylindrical shell of uniform thickness h, inner radius a_0 and outer radius a_q with variable material properties suspended in and filled with ideal compressible fluid mediums, and insonified by a time-harmonic plane acoustic wave normal to the axial direction (Fig. 1). Adopting a laminate model [16,17], the functionally graded shell is assumed to be composed of q layers of homogeneous isotropic materials, which are perfectly bonded at their interfaces and lined up such that their axes of symmetry coincide with each other (Fig. 1). The material properties within each layer of inner radius a_{j-1}, outer radius a_j and uniform thickness $h_j = a_j - a_{j-1}$ may described by the simple rule of mixture as [16,17,59,60]

$$\begin{aligned} \lambda_s^{[j]} &= V_F(\bar{r}_j)\lambda_s^{[1]} + \left[1 - V_F(\bar{r}_j)\right]\lambda_s^{[q]}, \\ \mu_s^{[j]} &= V_F(\bar{r}_j)\mu_s^{[1]} + \left[1 - V_F(\bar{r}_j)\right]\mu_s^{[q]}, \\ \rho_s^{[j]} &= V_F(\bar{r}_j)\rho_s^{[1]} + \left[1 - V_F(\bar{r}_j)\right]\rho_s^{[q]}, \end{aligned} \tag{11}$$

where $\bar{r}_j = (a_j + a_{j-1})/2$ $(j = 1, \ldots, q)$, and $(\lambda_s^{[j]}, \mu_s^{[j]})$, $\rho_s^{[j]}$, and $V_F(\bar{r}_j)$ are the Lame constants, mass density, and volume fraction of constituting material in the jth layer of the multilayered shell, respectively. Furthermore, the relevant scalar potentials corresponding to the compressional and shear waves transmitted into the jth layer of multilayered shell may conveniently be represented in the form of infinite generalized Fourier series as [56]

$$\begin{aligned} \phi_j &= \sum_{n=0}^{\infty} \left[C_n^{[j]}(\omega) H_n^{(1)}(k_p^{[j]} r) + D_n^{[j]}(\omega) H_n^{(2)}(k_p^{[j]} r) \right] \cos(n\theta), \\ \psi_j &= \sum_{n=1}^{\infty} \left[E_n^{[j]}(\omega) H_n^{(1)}(k_s^{[j]} r) + G_n^{[j]}(\omega) H_n^{(2)}(k_s^{[j]} r) \right] \sin(n\theta), \end{aligned} \tag{12}$$

where $H_n^{(2)}(x) = J_n(x) - \mathrm{i}\,Y_n(x)$ is the cylindrical Hankel function of the second kind of order n [57], and $C_n^{[j]}$ through $G_n^{[j]}$ are unknown transmission coefficients which will be determined later by imposing the appropriate boundary conditions.

4. Method of solution (*T*-matrix approach)

The specific steps taken in constructing the model for making use of the transfer matrix solution technique are described as follows [54]. After constructing the formal solution for the relevant field variables (i.e., stresses and displacements) associated with each layer in the multilayered (functionally graded) cylindrical shell in terms of scattering and transmission coefficients, these solutions are specialized to the outer and inner interfaces of the layer. Subsequently, the local transfer matrix for each layer is constructed by elimination of the common transmission coefficients. Such a matrix relation can be used, in conjunction with satisfying appropriate interface conditions across neighbouring layers, to directly relate the field variables of the inner face of one layer to the outer face of its outer neighbour. When this procedure is carried out consecutively for all layers in the bundle, a global transfer matrix (i.e., the product of the individual transfer matrixes) results, which connects the boundary variables at the outer and inner surfaces of the multilayered shell. In this way, the noble advantage of using the global transfer matrix saves us from tedious implementation of the boundary conditions at all $q+1$ interfaces (i.e., only the boundary conditions on the first and the last interface need to be imposed). Consequently, substitution of the scalar potentials (12) into the constitutive relations (9) and (10), leads to the matrix form of the formal solutions for the field variables (stress and displacement components) associated with the jth layer [54], i.e.,

$$\mathbf{W}_n^{[j]} = \mathbf{Q}_n^{[j]}\mathbf{X}_n^{[j]}, \tag{13}$$

where

$$\mathbf{W}_n^{[j]} = \left[\sigma_{rr,n}^{[j]}, \sigma_{r\theta,n}^{[j]}, u_{r,n}^{[j]}, u_{\theta,n}^{[j]}\right]^{\mathrm{T}}, \quad \mathbf{X}_n^{[j]} = \left[C_n^{[j]}, D_n^{[j]}, E_n^{[j]}, G_n^{[j]}\right]^{\mathrm{T}} \tag{14}$$

in which the elements of the coefficient matrix $\mathbf{Q}_n^{[j]}$ are given in Appendix A, and the stress and displacement components in the jth layer are expressed as

$$\begin{aligned}
\sigma_{rr}^{[j]}(r,\theta,\omega) &= \sum_{n=0}^{\infty} \sigma_{rr,n}^{[j]}(r,\omega)\cos(n\theta),\\
\sigma_{r\theta}^{[j]}(r,\theta,\omega) &= \sum_{n=1}^{\infty} \sigma_{r\theta,n}^{[j]}(r,\omega)\sin(n\theta),\\
u_{r}^{[j]}(r,\theta,\omega) &= \sum_{n=0}^{\infty} u_{r,n}^{[j]}(r,\omega)\cos(n\theta),\\
u_{\theta}^{[j]}(r,\theta,\omega) &= \sum_{n=1}^{\infty} u_{\theta,n}^{[j]}(r,\omega)\sin(n\theta).
\end{aligned} \tag{15}$$

The matrix relation (13) can advantageously be specialized for the inner and outer radii $r = \mathrm{a}_j, \mathrm{a}_{j-1}$ of the jth layer as

$$\mathbf{W}_n^{[j+]} = \mathbf{Q}_n^{[j+]}\mathbf{X}_n^{[j]}, \quad \mathbf{W}_n^{[j-]} = \mathbf{Q}_n^{[j-]}\mathbf{X}_n^{[j]}, \tag{16}$$

where the superscripts $[j+]$ and $[j-]$ denote the quantities evaluated at $r = \mathrm{a}_j$ and a_{j-1}, respectively. The above equations can be supplemented with the continuity conditions between each interface layer, i.e., $\mathbf{W}_n^{[j+]} = \mathbf{W}_n^{[(j+1)-]}$ at $r = \mathrm{a}_j$. Next, by eliminating the common amplitude vector $\mathbf{X}^{[j]}$ in Eq. (16), the field variable vector $\mathbf{W}_n^{[j+]}$ may be related to $\mathbf{W}_n^{[j-]}$ by

$$\mathbf{W}_n^{[j+]} = \mathbf{M}_n^{[j]}\mathbf{W}_n^{[j-]}, \tag{17}$$

where $\mathbf{M}_n^{[j]} = \mathbf{Q}_n^{[j+]}[\mathbf{Q}_n^{[j-]}]^{-1}$ is the local transfer matrix for jth layer, which relates the field variables at its outer surface to those at the inner surface. Subsequently, by invoking the continuity conditions between all interface

layers, the field variables at the outer radius of the total system, $r = a_q$, is related to those at the inner radius, $r = a_0$, via a 4×4 global transfer matrix, $\mathbf{T}_n$, by

$$\mathbf{W}_n^{[q+]} = \mathbf{T}_n \mathbf{W}_n^{[1-]}, \tag{18}$$

where

$$\mathbf{T}_n = \mathbf{M}_n^{[q]} \mathbf{M}_n^{[q-1]} \cdots \mathbf{M}_n^{[1]}. \tag{19}$$

The unknown coefficients A_n and B_n and the elements of the field variable vector, $\mathbf{W}_n^{[1-]}$, can be determined from the appropriate boundary conditions imposed at the inner ($r = a_0$) and the outer ($r = a_q$) surfaces of the multilayered shell. Thus, assuming continuity of normal fluid and solid velocities, normal stress and fluid pressure, and vanishing of tangential stress at $r = a_0$ and a_q implies that [53]

$$\begin{aligned} &(-i\omega) u_r(r,\theta,\omega)\big|_{r=a_0,a_q} = \mathbf{v}_r(r,\theta,\omega)\big|_{r=a_0,a_q}, \\ &\sigma_{rr}(r,\theta,\omega)\big|_{r=a_0,a_q} = -p(r,\theta,\omega)|_{r=a_0,a_q}, \\ &\sigma_{r\theta}(r,\theta,\omega)\big|_{r=a_0,a_q} = 0. \end{aligned} \tag{20}$$

Finally, making use of Eqs. (4) and (19)4a,4b,19 in Eq. (20), we obtain

$$-i\omega\left[T_n^{3,1}\sigma_{rr,n}^{[1-]} + T_n^{3,2}\sigma_{r\theta,n}^{[1-]} + T_n^{3,3}u_{r,n}^{[1-]} + T_n^{3,4}u_{\theta,n}^{[1-]}\right] + k_1\varepsilon_n i^n H'^{(1)}_n(k_1 a_q) A_n(\omega) = -\varphi_0 k_1 \varepsilon_n i^n J'_n(k_1 a_q), \tag{21a}$$

$$-i\omega u_{r,n}^{[1-]} + k_2 \varepsilon_n i^n J'_n(k_2 a_0) B_n(\omega) = 0, \tag{21b}$$

$$T_n^{1,1}\sigma_{rr,n}^{[1-]} + T_n^{1,2}\sigma_{r\theta,n}^{[1-]} + T_n^{1,3}u_{r,n}^{[1-]} + T_n^{1,4}u_{\theta,n}^{[1-]} - \omega\rho_1\varepsilon_n i^{n+1} H_n^{(1)}(k_1 a_q) A_n(\omega) = \omega\rho_1\varphi_0\varepsilon_n i^{n+1} J_n(k_1 a_q), \tag{21c}$$

$$\sigma_{rr,n}^{[1-]} + \omega\rho_2\varepsilon_n i^{n+1} J_n(k_2 a_0) B_n(\omega) = 0, \tag{21d}$$

$$T_n^{2,1}\sigma_{rr,n}^{[1-]} + T_n^{2,2}\sigma_{r\theta,n}^{[1-]} + T_n^{2,3}u_{r,n}^{[1-]} + T_n^{2,4}u_{\theta,n}^{[1-]} = 0, \tag{21e}$$

$$\sigma_{r\theta,n}^{[1-]} = 0. \tag{21f}$$

5. The global and resonance scattering coefficients

The most relevant field quantities associated with acoustic resonance scattering are the global and resonance scattering coefficients. The global scattering coefficient may be obtained from the standard definition of the backscattering form-function amplitude, which is written as [47,56]

$$|f_\infty(\theta = \pi, \omega)| \approx \lim_{r\to\infty} \sqrt{\frac{2r}{a_q}} \left|\frac{\varphi_1(r, \theta = \pi, \omega)}{\varphi_{\text{inc.}}}\right| = \left|\sum_{n=0}^{\infty} f_n(\theta = \pi, k_1 a_q)\right|, \tag{22}$$

where

$$f_n(\theta, k_1 a_q) = \frac{2\varepsilon_n}{\sqrt{\pi i k_1 a_q}} A_n \cos(n\theta) \tag{23}$$

is referred to as the global scattering coefficient for the nth mode. Consequently, the pure resonances in the scattering amplitudes of the nth normal mode can be isolated by subtracting the inherent backgrounds from the global form function as follows [47]:

$$\left|f_n^{(\text{res})}(\theta = \pi, k_1 a_q)\right| = \left|f_n(\theta = \pi, k_1 a_q) - f_n^{(b)}(\theta = \pi, k_1 a_q)\right|, \tag{24}$$

where the inherent background coefficients are defined as

$$f_n^{(b)}(\theta, k_1 a_q) = \frac{2\varepsilon_n}{\sqrt{\pi i k_1 a_q}} A_n^{(b)} \cos(n\theta), \tag{25}$$

here the background scattering coefficient, $A_n^{(b)}$, which is determined by solving the problem of interaction of a plane acoustic wave with an analogous multilayered fluid shell structure (i.e., by setting the transverse wave speeds in all of the solid layers equal to zero), is defined as [47]

$$A_n^{(b)} = (-1)\frac{k_1 a_q J_n'(k_1 a_q) - [F_n(0^+)]_q J_n(k_1 a_q)}{k_1 a_q H_n^{(1)'}(k_1 a_q) - [F_n(0^+)]_q H_n^{(1)}(k_1 a_q)}. \tag{26}$$

Here, the superscript "b" denotes the acoustical background and $[F_n(0^+)]_q$ is the zero limit of the accelerance function associated with the outer (qth) layer of the multilayered shell structure that, for the $n = 0$ mode, can be obtained through the following recurrence relation [47,61]

$$\begin{cases} [F_0(0^+)]_0 = \dfrac{4\rho_s^{[2]}}{\rho_2 - 4\rho_s^{[1]}\ln(1-h_1)}, \\ [F_0(0^+)]_j = \dfrac{\rho_s^{[j+1]}}{\rho_s^{[j]}} \dfrac{[F_0(0^+)]_{j-1}}{\left[1 - \ln(1-h_j)[F_0(0^+)]_{j-1}\right]}, \\ [F_0(0^+)]_q = \dfrac{\rho_1}{\rho_s^{[q]}} \dfrac{[F_0(0^+)]_{q-1}}{\left[1 - \ln(1-h_q)[F_0(0^+)]_{q-1}\right]}, \end{cases} \tag{27a}$$

where $j = 1, 2, \ldots, (q-1)$, and similarly for the $n \geqslant 1$ modes

$$\begin{cases} [F_n(0^+)]_0 = \dfrac{\rho_s^{[1]}}{\rho_2} n, \\ [F_n(0^+)]_j = \dfrac{\rho_s^{[j+1]} n^2 + l_j [F_n(0^+)]_{j-1}}{\rho_s^{[j]} \; l_j + [F_n(0^+)]_{j-1}}, \\ [F_n(0^+)]_q = \dfrac{\rho_1 \, n^2 + l_q [F_n(0^+)]_{q-1}}{\rho_s^{[q]} \; l_q + [F_n(0^+)]_{q-1}} \end{cases} \tag{27b}$$

in which $l_j = n(1 + (1-h_j)^{2n})/(1 - (1-h_j)^{2n})$ and $j = 1, 2, \ldots, (q-1)$. This completes the necessary background required for the exact resonance scattering analysis of a functionally graded cylindrical shell in an acoustic medium. Next, we consider some numerical examples.

6. Numerical results

In order to illustrate the nature and general behaviour of the solution, we consider some numerical examples. Realizing the large number of parameters involved here while keeping in view our computing hardware limitations, we confine our attention to a particular model. The surrounding and filling fluids are respectively assumed to be water ($\rho_1 = 1000\,\mathrm{kg/m^3}$, $c_1 = 1480\,\mathrm{m/s}$) and air ($\rho_2 = 1.2\,\mathrm{kg/m^3}$, $c_2 = 344\,\mathrm{m/s}$) at atmospheric pressure and ambient temperature. The cylindrical shell(total thickness $h/a_q = 0.1$) is assumed to be three-layered in which the interlayer (thickness $h_I = h_2 + h_3 + \cdots + h_{q-1}$) is graded in the radial direction with varying proportions of metallic aluminium (Al) substrate (thickness h_1) and ceramic zirconia (ZrO_2) coating (thickness h_q). The volume fraction of metal in the FGM interlayer is varied from 100% on the inner interface (at $r = a_0 + h_1 = a_1$) to zero on the outer interface (at $r = a_0 + h_1 + h_I = a_{q-1}$). Three special cases are considered. In the first case (case I), the Al substrate and the ZrO_2 coating are assumed to be absent (i.e., we have a single layer functionally graded cylindrical shell; $h_1 = h_q = 0$, $h_I/h = 1$). In the second case (case II) the thickness of the FGM mid-layer is supposed to be 50% of the total shell thickness ($h_1/h = h_q/h = 0.25$, $h_I/h = 0.5$), while in the third situation (case III) it is assumed to be only 10% of the total shell thickness ($h_1/h = h_q/h = 0.45$, $h_I/h = 0.1$). Furthermore, five distinct gradient profiles for the functionally graded interphase are studied in each case. Also, the volume fraction of Al in $a_1 \leqslant r \leqslant a_{q-1}$ for these situations

are assumed as follows:

$$V_F(r) = \left(1 - \frac{r - a_1}{h_I}\right)^{\gamma} \quad \text{where} \quad \begin{cases} \gamma = 0.2 & \text{metal rich (MR),} \\ \gamma = 1.0 & \text{linear (LN),} \\ \gamma = 5.0 & \text{ceramic rich (CR),} \end{cases} \tag{28a}$$

and

$$V_F(r) = \begin{cases} \dfrac{1}{2} + \dfrac{1}{2}\left[1 - \dfrac{2(r - a_1)}{h_I}\right]^{\gamma}, & a_1 < r < a_1 + (h_I/2), \\ \dfrac{1}{2} - \dfrac{1}{2}\left[\dfrac{2(r - a_1)}{h_I} - 1\right]^{\gamma}, & a_1 + (h_I/2) < r < a_{q-1}, \end{cases} \tag{28b}$$

where $\gamma = 0.2$ for sigmoidal1 (SM1) and $\gamma = 5$ for sigmoidal2 (SM2) profiles. The corresponding variations in volume fraction of Al along the radial axis are shown in Fig. 2. It is clear that MR simulates a metal-rich (MR) profile, CR a ceramic-rich profile, LN a linear profile, and SM1 and SM2 refer to sigmoidal compositions in the FGM interlayer. The latter design is desirable in situations where an MR composition near the inner interface and a CR near the outer interface is required. Also, due to the changes in the relative proportions of ZrO_2 and Al, elastic properties of the graded layer should also vary across its thickness. The effective structural properties of the interlayer can be determined by physical properties and volume fraction of the constituents (see Table 1) [62].

An MATLAB code was constructed for computing the global transfer matrix, $\mathbf{T}_n$, treating boundary conditions and to calculate the unknown scattering coefficients, and the global and the inherent background coefficients as functions of the non-dimensional frequency $k_1 a_q$ for a unit amplitude incident plane wave ($\varphi_0 = 1$). The computations were performed on a Pentium IV personal computer with a maximum number of layers $q_{\max} = 100$, a maximum truncation constant of $n_{\max} = 50$, especially selected to assure convergence in

Table 1
Material properties of the constituents

Material	ρ_s (kg/m^3)	λ_s (GPa)	μ_s (GPa)
Aluminium (Al)	2706	57.09	26.69
Zirconia (ZrO_2)	5700	129	94.8

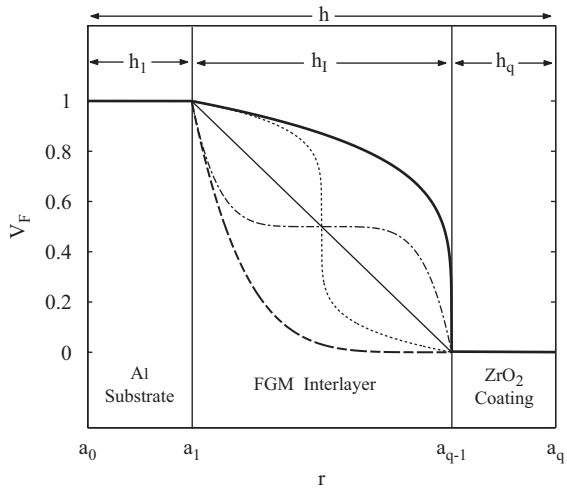

Fig. 2. The variations in volume fraction of aluminium in the FGM interlayer. (——— MR; —— LN; - - - - - - CR; – · – · – SM2; ····· SM1).

case of a thick FGM interlayer and also in the high-frequency range. The convergence was systematically checked in a simple trial and error manner, by increasing the number of layers, q, as well as the truncation constant (i.e., by including more modes in all summations) while looking for steadiness or stability in the numerical value of the solutions.

Fig. 3 shows the variations of the inherent background coefficient, $|f_n^{(b)}(\theta=\pi, k_1 a_q)|$, with dimensionless frequency, $k_1 a_q$, for case I (a single-layer FGM shell) with selected material gradient profiles (i.e., MR, LN, CR). The inherent background coefficients associated with a rigid cylinder and also a soft cylinder are shown for comparison purposes [30]. The rigid background is suitable for isolating the resonances of a very dense (heavy) cylinder, while the soft background has proved useful in extracting the resonances of a low density cylinder. Clearly, when densities of the solid and fluid mediums are of the same order of magnitude, neither rigid nor soft backgrounds are applicable [31]. In cases where the impedance ratio is close to unity, the proper background behaves intermediately between the rigid and soft backgrounds. We also note that results corresponding to the sigmoidal (SM1, SM2) profiles are not presented as they exhibit a very similar behaviour to that of the LN profile. This may be explained by the fact that the overall values of volume fractions of Al or ZrO_2 in the interphase region are very close in these situations. The most important observations are as follows. Since the FGM shell will appear "thin" to sound of long wavelength (small values of $k_1 a_q$) but "thick" to sound of short wavelength (large values of $k_1 a_q$), as expected, the character of the background coefficients will strongly depends on the acoustic wavelength in such a way that they approach the soft amplitude for $k_1 a_q \to 0$, and the rigid amplitude for $k_1 a_q \to \infty$. In particular, at very low frequencies, the "not so much thick" air-filled FGM shell appears to the incident wave simply as a cylindrical air bubble, which behaves essentially as a soft shell [30]. Consequently, at these frequencies, the inherent background coefficients associated with the LN, MR, CR profiles follow the soft background result fairly well. Furthermore, in the $n=0$ case (monopole mode), a notably high peak which is known in literature to be associated with the "giant monopole" resonance (i.e., analogous situation of air bubbles in water) is observed at a very low frequency [30]. Moreover, due to the relatively high thickness of the cylindrical shell ($h/a_q = 0.1$), the inherent background coefficient curves roughly follow the soft background curve (dotted line) in a very narrow band near the zero frequency. On the other hand, as the incident wave frequency increases, the inherent background coefficient curves begin to fairly well follow the rigid background curve (dash–dotted line). As the mode number increases, this correlation of background coefficients shifts to the higher frequencies, and the material composition (distribution profile) of the FGM shell appear to more effectively influence the modal background coefficients, especially at intermediate frequencies. Lastly, the inherent background coefficient curves corresponding to the CR gradient profile (dashed line) seem to be slightly shifted toward higher frequencies in comparison with that of the MR profile (thick solid line), mainly due to the increased overall rigidity of the CR composition. Also, for the same reason, the transition frequency (the frequency at which the inherent background undergoes from soft background to the rigid background) for CR shell is marked lower than that of the MR shell.

The first column in Fig. 4 shows the variations of the global scattering coefficient, $|f_n(\theta=\pi, k_1 a_q)|$, and the inherent background coefficient, $|f_n^{(b)}(\theta=\pi, k_1 a_q)|$, with dimensionless frequency for a double layer cylindrical shell, which consists of an Al inner layer and a ZrO_2 coating layer, at selected coating thickness ratios ($h_q/h = 0, 0.25, 0.75, 1$) for a fixed total shell thickness of $h/a_q = 0.1$. The second column in Fig. 4 shows the associated resonance scattering coefficients, $|f_n^{(\mathrm{res})}(\theta=\pi, k_1 a_q)|$, which are simply obtained by subtracting the inherent backgrounds from the global form functions. This can be used to illustrate that the elastic response consists of smooth background and resonance spectra. The difference in the two layered shell responses (e.g., compare $|f_n(\theta=\pi, k_1 a_q)|$ for $h_q/h = 0.25, 0.5, 0.75$) implies that the rigidities of these shells are different. The Al shell is the softest, while the Al shells with a ZrO_2 layer have a medium rigidity, and the ZrO_2 shell is the most rigid. In particular, the elastic responses of the two-layered shells are between those of the Al ($h_q/h = 0$) and ZrO_2 ($h_q/h = 1$) shells: the former is the low-frequency bound and the latter the high-frequency bound. This may be related to the fact that the circumferential waves corresponding to the resonances in ZrO_2 shell have faster phase speed than those in the Al shell. The global scattering coefficients perfectly coincide with the inherent background coefficients, except in the resonance region, where the resonances are very clearly isolated. As the partial wavenumber (mode number) n increases, the locations of the dominant resonance (peak) frequencies shift toward higher wavenumbers and some of the resonances are so weak that they hardly

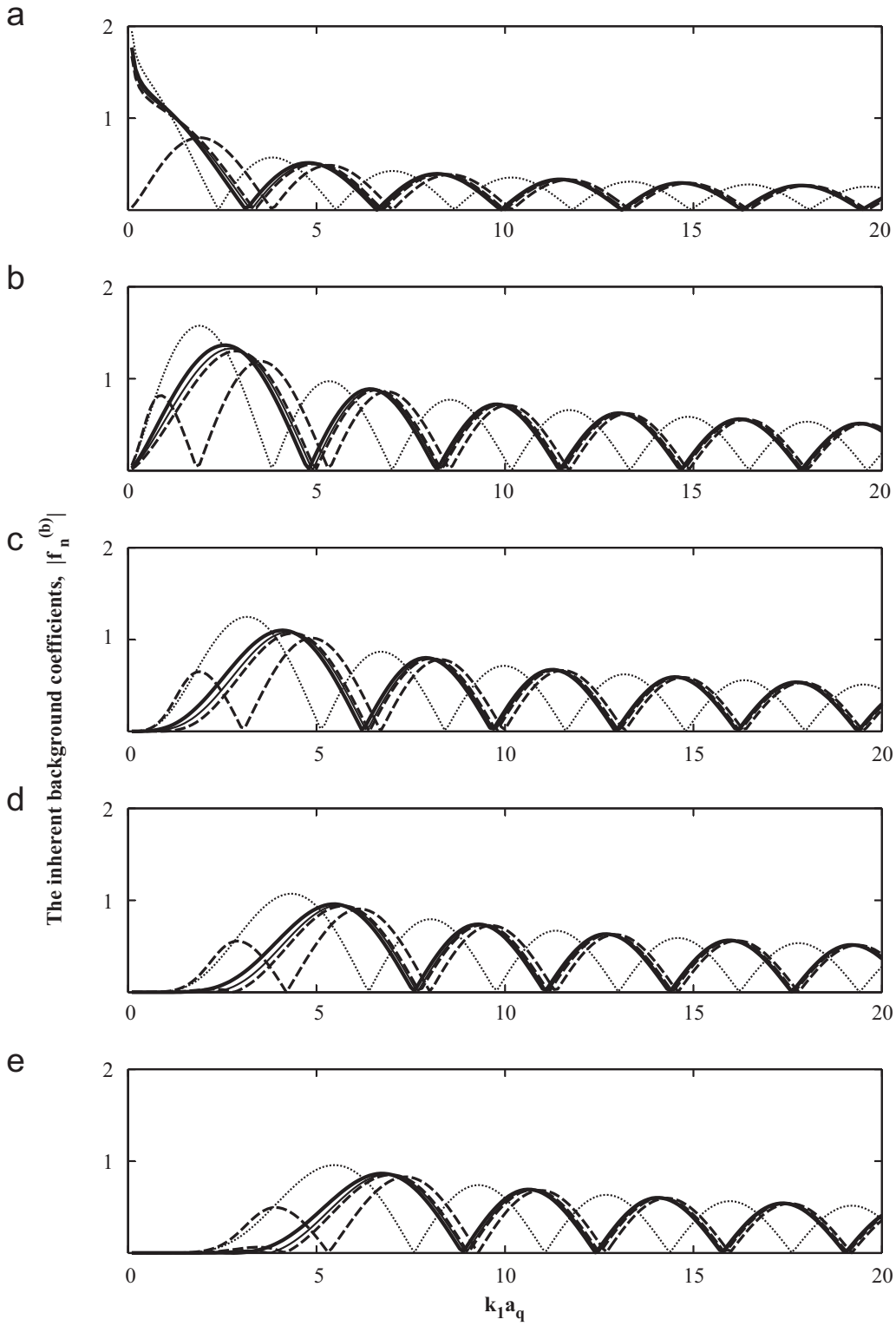

Fig. 3. The change in the inherent background coefficient with dimensionless frequency for selected mode number and compositional gradients: (a) $n = 0$, (b) $n = 1$, (c) $n = 2$, (d) $n = 3$, (e) $n = 4$ (——— MR; —— LN; - - - - - - CR; – · – · – rigid; ····· soft).

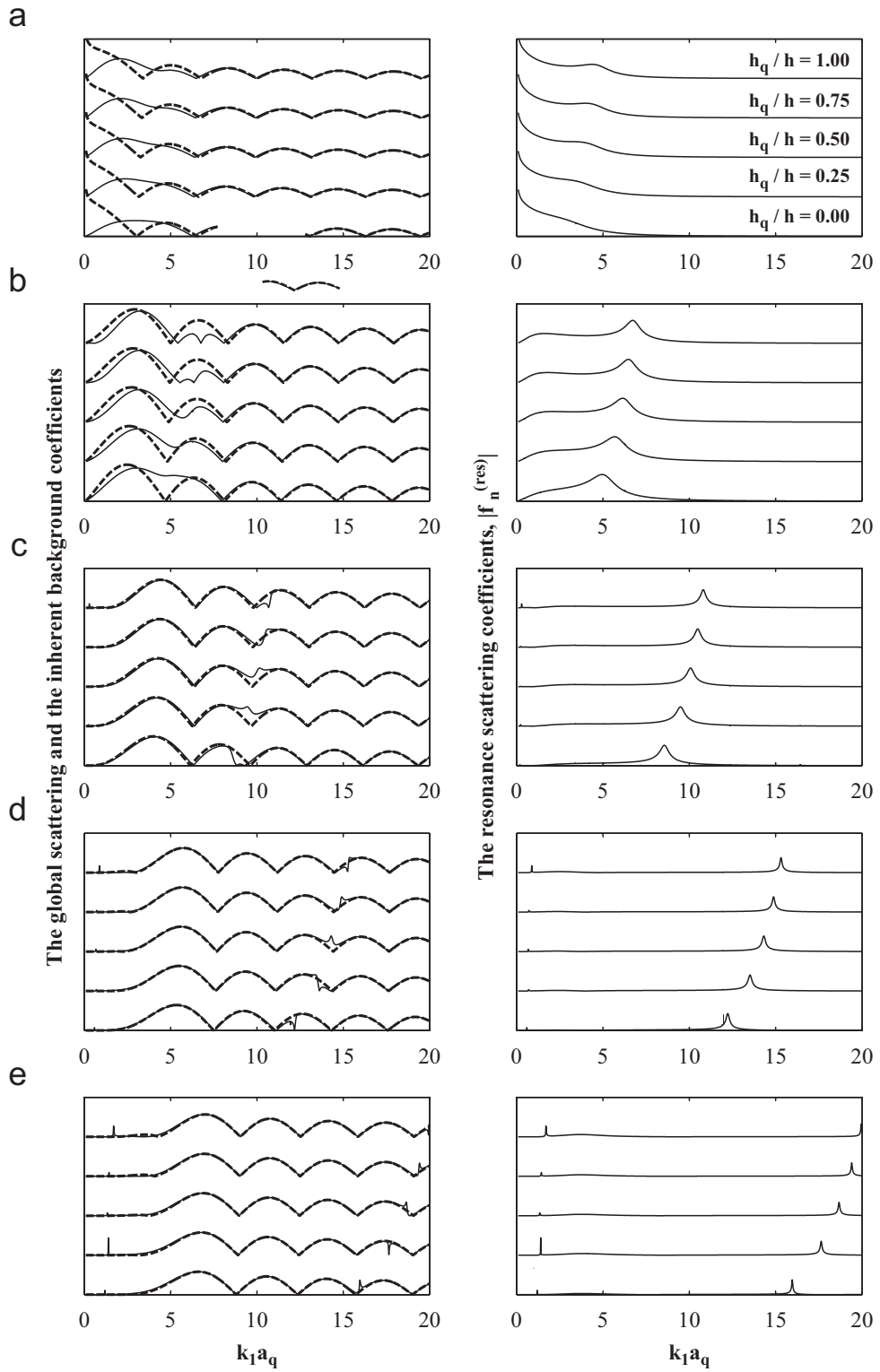

Fig. 4. The variation of the inherent background, global and resonance scattering coefficients with non-dimensional frequency for selected mode numbers and coating thickness ratios for a two-layer (ZrO_2/Al) cylindrical shell: (a) $n = 0$, (b) $n = 1$, (c) $n = 2$, (d) $n = 3$, (e) $n = 4$ (left column: —— global scattering coefficient; - - - - - - inherent background coefficient; —— right column: resonance scattering coefficient).

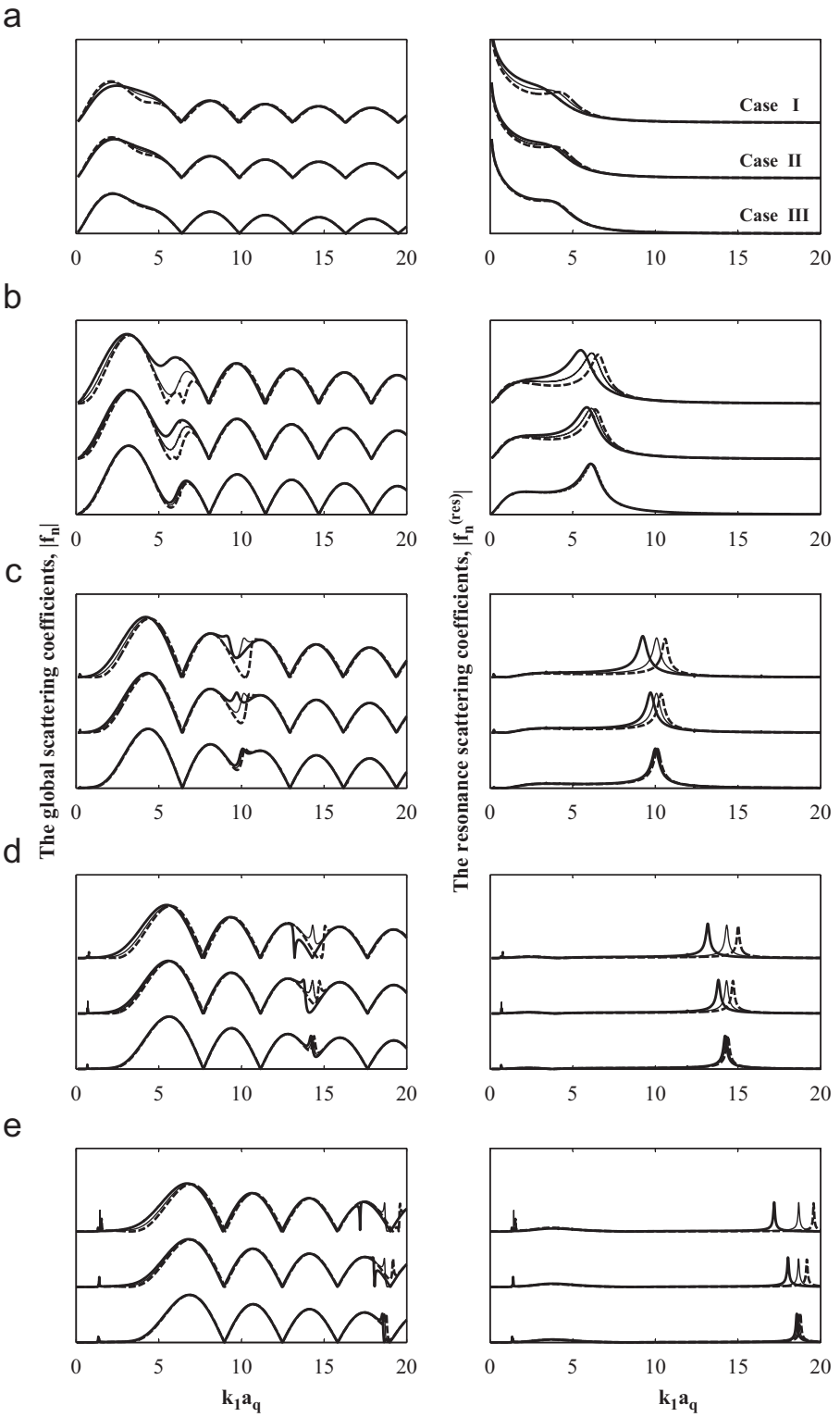

Fig. 5. The variation of the global and resonance scattering coefficients with non-dimensional frequency for selected mode numbers and FGM interlayer configurations; (a) $n = 0$, (b) $n = 1$, (c) $n = 2$, (d) $n = 3$, (e) $n = 4$ (——— MR; —— LN; - - - - - - CR).

appear in the spectrum (especially for $n = 2$, 3, 4 at relatively low frequencies). The resonance frequency associated with the single layer ZrO_2 shell ($h_q/h = 1$) is slightly higher than that of the Al shell ($h_q/h = 0$), and this difference increases as the mode number increases. Furthermore, the resonance frequency bandwidth associated with the single layer ZrO_2 shell is slightly narrower than that of the Al shell, especially for low mode numbers. The resonances of the two-layered shells have different characteristics of propagation and radiation damping. The dependence of the resonance frequencies on coating thickness can be observed more clearly with these resonance spectra than on the global scattering coefficients. In particular, as the waves penetrate into the compound shell, the entire structure of two-layered system is seen to affect both the frequency and the quality (amplitude and width) of the resonances in these spectra. The resonances corresponding to the higher mode numbers ($n > 2$), show higher sensitivity to the change in coating (ZrO_2) thickness. These variations are approximately LN and show monotonic behaviour. It can be shown that this monotonic behaviour and LN variation of resonances with change of coating thickness, is consistent with the dependence of phase velocities of surface waves corresponding to these resonances [63]. As a consequence, the characteristics of dominant resonances of the higher modes (i.e., location, amplitude and width) can be a good indicator of coating thickness.

Fig. 5 shows the variations of the global scattering coefficient and the associated resonance scattering coefficient with dimensionless frequency for selected Al/ZrO_2 gradient profiles (i.e., MR, LN, CR) and structural configurations (case I: a single FGM shell: $h_1 = h_q = 0$, $h_I/h = 1$; case II: a 50% FGM mid-layer $h_1/h = h_q/h = 0.25$, $h_I/h = 0.5$; case III: a 10% FGM mid-layer: $h_1/h = h_q/h = 0.45$, $h_I/h = 0.1$) for a given total shell thickness of $h/a_q = 0.1$. As before, the resonances can be readily isolated by using the inherent backgrounds for FGM cylindrical shells (see Fig. 3). The most important observations are as follows. As the thickness of the FGM interlayer increases, the difference between the scattering coefficients increases, especially for higher mode numbers. In particular, the dominant resonance frequencies corresponds to the MR profiles are (monotonically) shifted to the left toward the resonance frequency previously observed in Fig. 4 for a single-layer Al shell, while the quality (amplitude, bandwidth) of the resonances also tend to become similar to that of the Al shell, with increasing the thickness of FGM layer. Similarly, the dominant resonance frequencies corresponding to the CR profile are shifted to the right toward the resonance frequency for the single-layer ZrO_2 shell (see Fig. 4), while the quality (amplitude, bandwidth) of the resonances also tend to

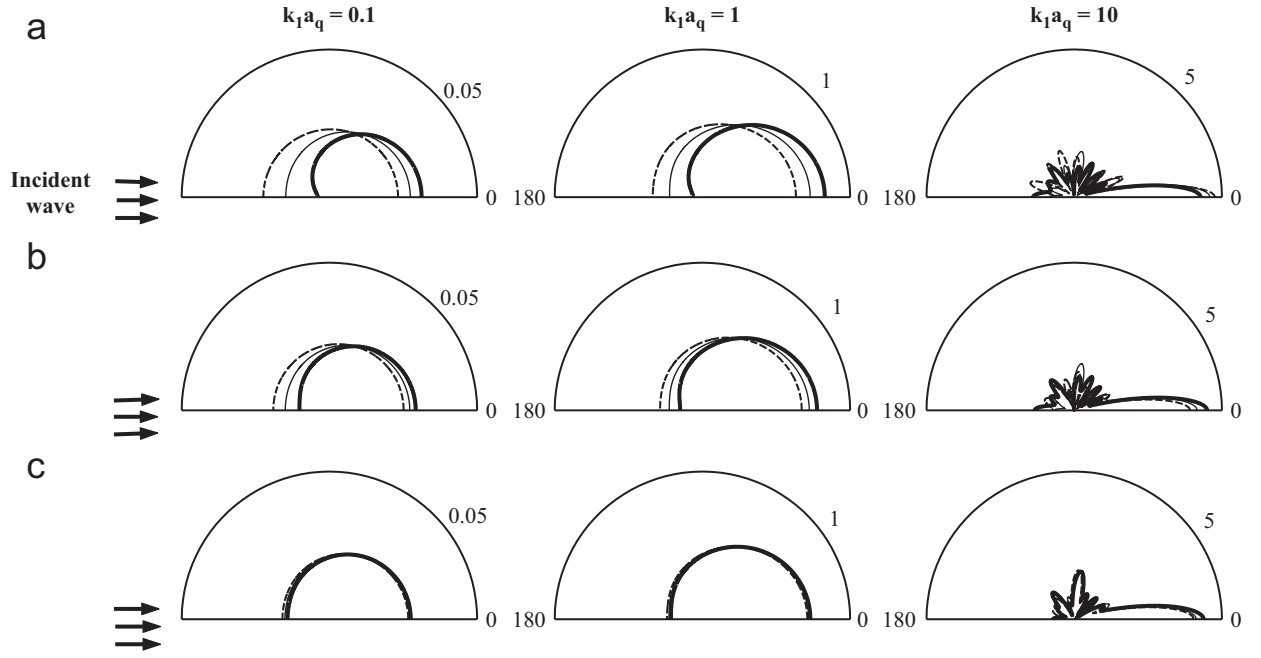

Fig. 6. The angular distribution of the far-field form function amplitude for selected wavenumbers and material gradient profiles: (a) case I, (b) case II, (c) case III (——— MR; —— LN; - - - - - - CR).

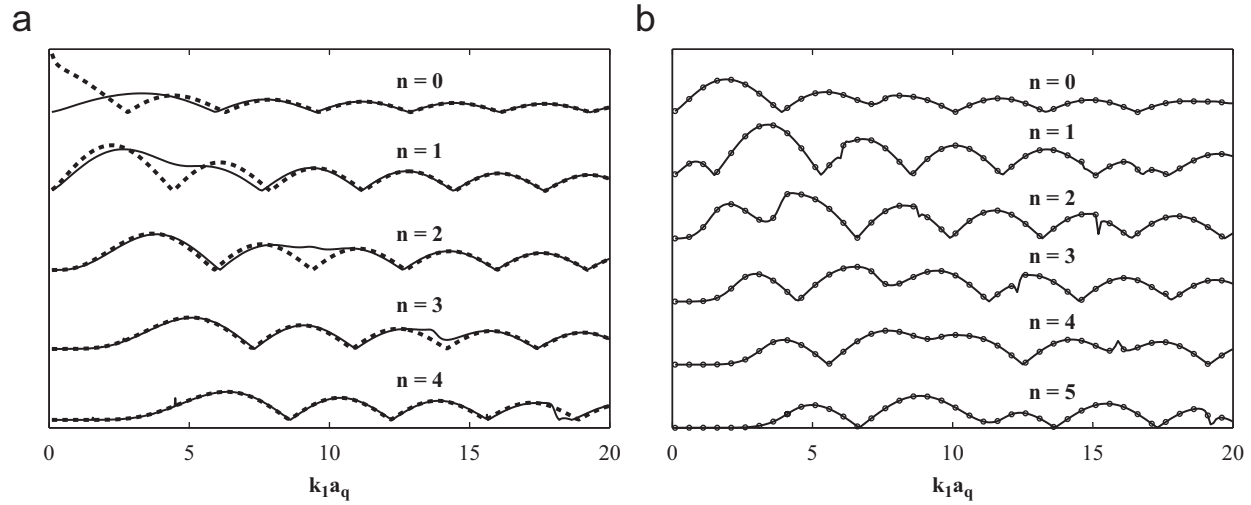

Fig. 7. (a) The variations of the global and inherent background coefficients with dimensionless frequency for selected mode numbers for a two-layered air-filled aluminium-tungsten carbide cylindrical shell submerged in water (—— global scattering coefficient; - - - - - - inherent background coefficients). (b) The change in the modal backscattering form function amplitude with dimensionless frequency for selected mode numbers for an air-filled aluminium shell submerged in water. (—— Murphy et al.'s results [25]; ○ multilayered Al shell, $q = 100$).

become similar to that of the ZrO_2 shell. Thus one can conclude that the gradient profile of the constituents have the most pronounced effects on the resonance spectra characteristic, especially for relative thick FGM interlayers (shells). We also note that the resonance frequencies associate with the constant LN profile do not appear to change position as the FGM interlayer thickness increases, which is clearly due to the fact that the constituent volume fractions remain constant across the interlayer thickness (i.e., 50% Al-50% ZrO_2) in this situation.

Fig. 6 displays the angular distribution of the far-field form function amplitude, $|f_\infty(\theta = \pi, \omega)|$, for the selected configurations (cases I, II, III) and material gradient profiles (LN, MR, CR) at specific wavenumbers ($k_1 a_q = 0.1,\ 1,\ 10$). The most important observations are as follows. Decreasing the thickness of FGM layer (i.e., cases II and III), leads to a notable decrease in the difference between the curves corresponding to different material composition profiles, especially in the forward ($\theta = 0$) direction. At low and intermediate frequencies ($k_1 a_q = 0.1, 1$), the form function directivities exhibit a very uniform pattern. This is due to the fact that, in contrast to the high frequency case ($k_1 a_q = 10$), the breathing ($n = 0$) and the rigid body ($n = 1$) modes are the dominant modes at these frequencies. Furthermore, the CR profile causes the largest (smallest) scattering amplitude in the backward (forward) direction, while for the MR (metal rich) profile the situation is reversed. At the highest frequency considered ($k_1 a_q = 10$), there is almost no difference observed between the profiles in the forward direction as all the curves nearly coincide in this direction, even for the thickest FGM interlayer (case I). Hence we may conclude that identification of material distribution profiles from the scattering amplitude measurements in the backward direction may be far more gainful than that in the forward direction, even for very thin interlayer at relatively high excitation frequencies. As a final observation, we note that maximum scattering amplitude occurs mainly in the backward direction for all three frequencies considered.

Finally, to check overall validity of the work, we computed the variations of the global scattering coefficient and the associated inherent background coefficient with dimensionless frequency for a two-layered air-filled aluminium (Al)-tungsten carbide (WC) 2%-thickness shell submerged in water by setting $h/a_q = 0.02$, $q = 2$, $\rho^{[1]}2790\,\mathrm{kg/m^3}$, $\lambda^{[1]} = 59.9\,\mathrm{GPa}$, $\mu^{[1]} = 26.8\,\mathrm{GPa}$, $\rho^{[2]} = 13{,}800\,\mathrm{kg/m^3}$, $\lambda^{[2]} = 166.0\,\mathrm{GPa}$, $\mu^{[2]} = 241.6\,\mathrm{GPa}$, $\rho_1 = 1000\,\mathrm{kg/m^3}$, $c_1 = 1480\,\mathrm{m/s}$, $\rho_2 = 1.2\,\mathrm{kg/m^3}$ and $c_2 = 340\,\mathrm{m/s}$ in our general MATLAB code. The numerical results, as shown in Fig. 7a show good agreement with those displayed in Fig. 11 of [47]. As a further check, we greatly increased the number of layers (i.e., set $q = 100$) in an FGM cylindrical shell (case I) and let $\gamma \to 0$ ($V_F \to 1$) in Eq. (28a) to compute the modal backscattering form function amplitude for

an air-filled single-layer aluminium shell submerged in water by setting $h/a_q = 0.8$, $q = 100$, $\rho^{[j]} = 2790\,\mathrm{kg/m^3}$, $\lambda^{[j]} = 59.7\,\mathrm{GPa}$, $\mu^{[j]} = 26.7\,\mathrm{GPa}$ (for $j = 1, 2, \ldots, 100$), and $\rho_1 = 1000\,\mathrm{kg/m^3}$, $c_1 = 1480\,\mathrm{m/s}$, $\rho_2 = 1.2\,\mathrm{kg/m^3}$ and $c_2 = 344\,\mathrm{m/s}$, in our general MATLAB code. The numerical results, as shown in Fig. 7b show good agreement with those displayed in Fig. 1 of Ref. [30].

7. Conclusions

The acoustic resonance characteristics of layered (FGM) shells can effectively be analysed by taking advantage of the inherent background coefficients. The pure resonances associated with the scattering amplitudes of the nth order partial wave can be isolated by subtracting the inherent backgrounds (non-resonance component) from the backscattering form function. The present work is concerned with acoustic wave interaction with a thick-walled three-layered cylindrical shell in which the coating phase is interfaced with the substrate shell through a functionally graded interlayer. The solution of the problem is derived by means of the very powerful transfer matrix method, which effectively reduces the order of the final solving matrix and greatly improves the computational precision. Special attention is paid to the influence of material compositional profiles in the graded region on the frequency spectrum of global, inherent background, and resonance scattering coefficients. Numerical results for a ZrO_2-coated Al shell with different variations of interlayer properties are presented and discussed. The computed results reveal that the background coefficients for the FGM cylindrical shell strongly depends on the acoustic wave length in such a way that they approach the soft background amplitude (e.g., behave like a cylindrical air bubble) at low incident wave frequencies, and toward the rigid background amplitude (e.g., behave like a rigid cylinder) at high frequencies. As the mode number increases, this correlation of background coefficients shifts to the higher frequencies, and the material compositional profile of the FGM shell appear to more effectively influence the modal background coefficients, especially at intermediate frequencies. It has also been found that for a relatively thick FGM Al/ZrO_2 interlayer, the gradient profile of the constituents have the most pronounced effects on the resonance spectra characteristics. In particular, the dominant resonance frequencies corresponding to the MR (CR) profiles are monotonically shifted to the left (right) toward the resonance frequency for a single-layer Al (ZrO_2) shell, while the quality of the resonances also tend to become similar to that of the single-layer Al (ZrO_2) shell. The resonance frequencies associated with the constant LN profile do not appear to change position as the FGM interlayer thickness increases. Furthermore, the far-field form function amplitude directivity patterns show that identification of material composition distribution profiles from the scattering amplitude measurements in the backward direction may be far more gainful than that in the forward direction, even for very thin interlayer at relatively high excitation frequencies. Finally, in case of a (two-layer) ZrO_2 coated Al shell, the sensitivity of the resonance frequencies and quality (amplitude and width) to coating thickness is illustrated. In particular, it has been demonstrated that the quality and characteristics of dominant resonances of the higher-order modes ($n > 2$) can be a good indicator of coating thickness.

Appendix A

$$
\begin{aligned}
Q_n^{[j]}(1,1) &= -\left[(\lambda_s^{[j]} + 2\mu_s^{[j]})(n^2 - n - k_p^{2[j]}r^2) + \lambda_s^{[j]} n(1-n)\right] H_n^{(1)}(k_p^{[j]}r) - 2\mu_s^{[j]} k_p^{[j]} r H_{n+1}^{(1)}(k_p^{[j]}r),\\
Q_n^{[j]}(1,2) &= -\left[(\lambda_s^{[j]} + 2\mu_s^{[j]})(n^2 - n - k_p^{2[j]}r^2) + \lambda_s^{[j]} n(1-n)\right] H_n^{(2)}(k_p^{[j]}r) - 2\mu_s^{[j]} k_p^{[j]} r H_{n+1}^{(2)}(k_p^{[j]}r),\\
Q_n^{[j]}(1,3) &= -2\mu_s^{[j]} n\left[(n-1)H_n^{(1)}(k_s^{[j]}r) - k_s^{[j]} r H_{n+1}^{(1)}(k_s^{[j]}r)\right],\\
Q_n^{[j]}(1,4) &= -2\mu_s^{[j]} n\left[(n-1)H_n^{(2)}(k_s^{[j]}r) - k_s^{[j]} r H_{n+1}^{(2)}(k_s^{[j]}r)\right],\\
Q_n^{[j]}(2,1) &= 2\mu_s^{[j]}\left[H_n^{(1)}(k_p^{[j]}r) n(n-1) - n k_p^{[j]} r H_{n+1}^{(1)}(k_p^{[j]}r)\right],\\
Q_n^{[j]}(2,2) &= 2\mu_s^{[j]}\left[H_n^{(2)}(k_p^{[j]}r) n(n-1) - n k_p^{[j]} r H_{n+1}^{(2)}(k_p^{[j]}r)\right],
\end{aligned}
$$

$$Q_n^{[j]}(2,3) = \mu_s^{[j]}\left[H_n^{(1)}(k_s^{[j]}r)(2n(n-1) - k_s^{2[j]}r^2) + 2k_s^{[j]}rH_{n+1}^{(1)}(k_s^{[j]}r)\right],$$

$$Q_n^{[j]}(2,4) = \mu_s^{[j]}\left[H_n^{(2)}(k_s^{[j]}r)(2n(n-1) - k_s^{2[j]}r^2) + 2k_s^{[j]}rH_{n+1}^{(2)}(k_s^{[j]}r)\right],$$

$$Q_n^{[j]}(3,1) = -nH_n^{(1)}(k_p^{[j]}r) + k_p^{[j]}rH_{n+1}^{(1)}(k_p^{[j]}r),$$

$$Q_n^{[j]}(3,2) = -nH_n^{(2)}(k_p^{[j]}r) + k_p^{[j]}rH_{n+1}^{(2)}(k_p^{[j]}r),$$

$$Q_n^{[j]}(3,3) = -nH_n^{(1)}(k_s^{[j]}r),$$

$$Q_n^{[j]}(3,4) = -nH_n^{(2)}(k_s^{[j]}r),$$

$$Q_n^{[j]}(4,1) = nH_n^{(1)}(k_p^{[j]}r),$$

$$Q_n^{[j]}(4,2) = nH_n^{(2)}(k_p^{[j]}r),$$

$$Q_n^{[j]}(4,3) = nH_n^{(1)}(k_s^{[j]}r) - k_s^{[j]}rH_{n+1}^{(1)}(k_s^{[j]}r),$$

$$Q_n^{[j]}(4,4) = nH_n^{(2)}(k_s^{[j]}r) - k_s^{[j]}rH_{n+1}^{(2)}(k_s^{[j]}r).$$

References

[1] M. Yamanouchi, M. Koizumi, T. Hirai, I. Shiota, *Proceedings of the First International Symposium on Functionally Gradient Materials*, Sendai, Japan, 1990.

[2] J.B. Holt, M. Koizumi, T. Hirai, Z.A. Munir, *Ceramic Transaction: Functionally Gradient Materials*, Vol. 34, The American Ceramic Society, OH, Westerville, 1993.

[3] M. Koizumi, The concept of FGM, in: J.B. Holt, M. Koizumi, T. Hirai, Z.A. Munir (Eds.), *Ceramic Transaction: Functionally Gradient Materials*, Vol. 34, The American Ceramic Society, Ohio, Westerville, 1993, pp. 3–10.

[4] S. Suresh, A. Mortensen, *Fundamentals of Functionally Graded Materials*, IOM Communications, London, 1998.

[5] Y. Miyamoto, W.A. Kaysser, B.H. Rabin, A. Kawasaki, R.G. Ford, *Functionally Graded Materials: Design, Processing and Applications*, Chapman & Hall, 1999.

[6] C.T. Loy, K.Y. Lam, J.N. Reddy, Vibration of functionally graded cylindrical shells, *International Journal of Mechanical Sciences* 41 (1999) 309–324.

[7] S.C. Pradhan, C.T. Loy, K.Y. Lam, J.N. Reddy, Vibration characteristics of functionally graded cylindrical shells under various boundary conditions, *Applied Acoustics* 29 (2000) 61–111.

[8] S.W. Gong, K.Y. Lam, J.N. Reddy, The elastic response of functionally graded cylindrical shells to low-velocity impact, *International Journal of Impact Engineering* 22 (1999) 397–417.

[9] T.Y. Ng, K.M. Lam, K.M. Liew, J.N. Reddy, Dynamic stability analysis of functionally graded cylindrical shells under periodic axial loading, *International Journal of Solids and Structures* 38 (2001) 1295–1309.

[10] X. Han, G.R. Liu, Z.C. Xi, K.Y. Lam, Transient waves in a functionally graded cylinder, *International Journal of Solids and Structures* 38 (2001) 3021–3037.

[11] X. Han, G.R. Liu, Elastic waves in a functionally graded piezoelectric cylinder, *Smart Materials and Structures* 12 (2003) 962–971.

[12] X. Han, D. Xu, G.R. Liu, Transient responses in a functionally graded cylindrical shell to a point load, *Journal of Sound and Vibration* 251 (2002) 783–805.

[13] J. Yang, H.S. Shen, Free vibration and parametric resonance of shear deformable functionally graded cylindrical panels, *Journal of Sound and Vibration* 261 (2003) 871–893.

[14] A.H. Sofiyev, Dynamic buckling of functionally graded cylindrical thin shells under non-periodic impulsive loading, *Acta Mechanica* 165 (2003) 151–163.

[15] A.H. Sofiyev, The stability of compositionally graded ceramic-metal cylindrical shells under aperiodic axial impulsive loading, *Composite Structures* 69 (2005) 247–257.

[16] W.Q. Chen, Z.G. Bian, H.J. Ding, Three-dimensional vibration analysis of fluid-filled orthotropic FGM cylindrical shells, *International Journal of Mechanical Sciences* 46 (2004) 159–171.

[17] W.Q. Chen, Z.G. Bian, C.F. Lv, H.J. Ding, 3D free vibration analysis of a functionally graded piezoelectric hollow cylinder filled with compressible fluid, *International Journal of Solids and Structures* 41 (2004) 947–964.

[18] L. Elmaimouni, J.E. Lefebvre, V. Zhang, T. Gryba, Guided waves in radially graded cylinders: a polynomial approach, *NDT&E International* 38 (2005) 344–353.

[19] J.Q. Zhu, C. Chen, Y.P. Shen, S.L. Wang, Dynamic stability of functionally graded piezoelectric circular cylindrical shells, *Materials Letters* 59 (2005) 477–485.

[20] B.P. Patel, S.S. Gupta, M.S. Loknath, C.P. Kadu, Free vibration analysis of functionally graded elliptical cylindrical shells using higher-order theory, *Composite Structure* 69 (2005) 259–270.

[21] R. Kadoli, N. Ganesan, Buckling and free vibration analysis of functionally graded cylindrical shells subjected to a temperature-specified boundary condition, *Journal of Sound and Vibration* 289 (2006) 450–480.
[22] J.L. Pelletier, S.S. Vel, An exact solution for the steady-state thermoelastic response of functionally graded orthotropic cylindrical shells, *International Journal of Solids and Structures* 43 (2006) 1131–1158.
[23] M. Shakeri, M. Akhlaghi, S.M. Hoseini, Vibration and radial wave propagation velocity in functionally graded thick hollow cylinder, *Composite Structures* 76 (2006) 174–184.
[24] M. Talmant, H. Batard, Material characterization and resonant scattering by cylinders, *Proceedings of the IEEE Ultrasonics Symposium* 3 (1994) 1371–1380.
[25] A. Migliori, J.L. Sarrao, *Resonant ultrasound spectroscopy: applications to physics, Materials Measurements and Nondestructive Evaluation*, Wiley, New York, 1997.
[26] A. Tesei, W.L.J. Fox, A. Maguer, A. Lovik, Target parameter estimation using resonance scattering analysis applied to air-filled, cylindrical shells in water, *Journal of the Acoustical Society of America* 108 (2000) 2891–2910.
[27] D. Guicking, K. Goerk, H. Peine, Recent advances in sonar target classification, *Proceedings of SPIE—The International Society for Optical Engineering* 1700 (1995) 2–15.
[28] F. Honarvar, A.N. Sinclair, Nondestructive evaluation of cylindrical components by resonance acoustic spectroscopy, *Ultrasonic* 36 (1998) 845–854.
[29] L. Flax, L.R. Dragonette, H. Uberall, Theory of elastic resonance excitation by sound scattering, *Journal of the Acoustical Society of America* 63 (1978) 723–731.
[30] J.D. Murphy, E.D. Breitenbach, H. Uberall, Resonance scattering of acoustic waves from cylindrical shells, *Journal of the Acoustical Society of America* 64 (1978) 677–683.
[31] G.C. Gaunaurd, D. Brill, Acoustic spectrogram and complex-frequency poles of a resonantly excited elastic tube, *Journal of the Acoustical Society of America* 75 (1984) 1681–1693.
[32] J.L. Izbicki, G. Maze, J. Ripoche, Influence of the free modes of vibration on the acoustic scattering of a circular cylindrical shell, *Journal of the Acoustical Society of America* 80 (1986) 1215–1219.
[33] M. Talmant, G. Quentin, J.L. Rousselot, J.V. Subrahmanyam, H. Überall, Acoustic resonances of thin cylindrical shells and the resonance scattering theory, *The Journal of the Acoustical Society of America* 84 (1988) 681–688.
[34] N.D. Veksler, Analysis of peripheral waves in the problem of plane acoustic pressure wave scattering by a circular cylindrical shell, *Acustica* 69 (1989) 7–63.
[35] J.L. Izbicki, J.L. Rousselot, A. Gérard, G. Maze, J. Ripoche, Analysis of resonances related to Scholte–Stoneley waves around circular cylindrical shells, *The Journal of the Acoustical Society of America* 90 (1991) 2602–2608.
[36] G. Maze, F. Léon, N. Veksler, J. Ripoche, Influence of the incidence angle on the scattering by a circular cylindrical shell, *The Journal of the Acoustical Society of America* 95 (1994) 3000.
[37] G. Maze, F. Léon, F. Lecroq, D. Décultot, H. Überall, Scholte interface wave on a cylindrical shell, *The Journal of the Acoustical Society of America* 96 (1994) 3243.
[38] G. Kaduchak, C.M. Loeffler, Sound scattering by a fluid-filled cylindrical shell in water, *The Journal of the Acoustical Society of America* 97 (1995) 3423–3424.
[39] G. Maze, J.M. Conoir, F. Léon, D. Décultot, Acoustic scattering from a circular cylindrical shell excited by a short pulse in oblique incidence: helical waves, *The Journal of the Acoustical Society of America* 97 (1995) 3395.
[40] G. Liu, W. Tang, Purely elastic resonance scattering of an obliquely incident plane acoustic wave by a submerged cylindrical shell of infinite length, *Acta Acustica* 21 (1996) 805–814.
[41] J.P. Lee, J.H. Song, M.S. Choi, Effects of material attenuation on acoustic resonance scattering from cylindrical tubes, *Ultrasonics* 34 (1996) 737–745.
[42] N.D. Veksler, J.L. Izbicki, Modal resonances of peripheral waves, *Acta Acustica* 82 (1996) 401–410.
[43] G. Kaduchak, C.M. Loeffler, Backscattering of obliquely incident plane waves by a composite cylindrical shell constructed of isotropic and transversely isotropic layers, *The Journal of the Acoustical Society of America* 99 (1996) 2545–2574.
[44] M.S. Choi, Y.S. Joo, J.P. Lee, The inherent background in acoustic wave scattering by a submerged target, *The Journal of the Acoustical Society of America* 99 (1996) 2594–2603.
[45] M.S. Choi, Y.S. Joo, J.P. Lee, Inherent background coefficients for submerged cylindrical shells, *The Journal of the Acoustical Society of America* 101 (1997) 1743–1745.
[46] M.S. Choi, Y.S. Joo, Theory of the background amplitudes in acoustic resonance scattering, *The Journal of the Acoustical Society of America* 101 (1997) 2083–2087.
[47] Y.S. Joo, J.G. Ih, M.S. Choi, Inherent background coefficients for acoustic resonance scattering from submerged, multilayered, cylindrical structures, *The Journal of the Acoustical Society of America* 103 (1998) 900–910.
[48] J.M. Conoir, J.L. Izbicki, O. Lenoir, Phase gradient method applied to scattering by an elastic shell, *Ultrasonics* 35 (1997) 157–169.
[49] E. Kheddioui, J.M. Conoir, P. Pareige, J.L. Izbicki, Resonant scattering by two elastic cylindrical shells, *Acta Acustica* 84 (1998) 980–986.
[50] X.L. Bao, P.K. Raju, H. Überall, Circumferential waves on an immersed fluid-filled elastic cylindrical shell, *The Journal of the Acoustical Society of America* 105 (1999) 2704–2709.
[51] H. Überall, Acoustics of shells, *Acoustical Physics* 47 (2003) 115–139.
[52] J.Y. Kim, J.G. Ih, Scattering of plane acoustic waves by a transversely isotropic cylindrical shell-application to material characterization, *Applied Acoustics* 64 (2003) 1187–1204.

[53] Y. Fan, F. Honarvar, A.N. Sinclair, M.R. Jafari, Circumferential resonance modes of solid elastic cylinders excited by obliquely incident acoustic waves, *Journal of the Acoustical Society of America* 113 (2003) 102–113.
[54] A.H. Nayfeh, P.B. Nagy, General study of axisymmetric waves in layered anisotropic fibers and their composites, *Journal of the Acoustical Society of America* 99 (1996) 931–941.
[55] A.D. Pierce, *Acoustics: An Introduction to Its Physical Principles and Applications*, American Institute of Physics, New York, 1991.
[56] S.M. Hasheminejad, N. Safari, Acoustic scattering from viscoelastically coated spheres and cylinders in viscous fluids, *Journal of Sound and Vibration* 280 (2005) 101–125.
[57] M. Abramovitz, I.A. Stegun, *Handbook of Mathematical Functions*, National Bureau of Standards, Washington, DC, 1964.
[58] J.D. Achenbach, *Wave Propagation in Elastic Solids*, North-Holland, New York, 1976.
[59] H. Nozaki, Y. Shindo, Effect of interface layers on elastic wave propagation in a fiber-reinforced metal-matrix composite, *International Journal of Engineering Science* 36 (1998) 383–394.
[60] H. Sato, Y. Shindo, Diffraction of elastic waves by a circular inclusion with a nonhomogeneous interface layer and dynamic stress concentration, *Proceeding of the 48th Japan National Congress on Theoretical and Applied Mechanics*, 1999, pp. 81–94.
[61] M.S. Choi, Inherent background coefficient of the axisymmetric mode in acoustic resonance scattering from a system of multilayered shells, *Journal of the Korean Physical Society* 37 (2000) 519–526.
[62] G.N. Praveen, C.D. Chin, J.N. Reddy, Thermoelastic analysis of functionally graded ceramic-metal cylinder, *Journal of Engineering Mechanics* 125 (1999) 1259–1267.
[63] F. Honarvar, A.N. Sinclair, Scattering of an obliquely incident plane wave from a circular clad rod, *Journal of the Acoustical Society of America* 102 (1997) 41–48.